Efficient Preprocessing of Site-Specific Radio Channels for Virtual Drive Testing in Hardware Emulators

Mbugua, Allan Wainaina; Chen, Yun; RASCHKOWSKI, LESZEK; Ji, Yilin; GHARBA, MOHAMED; Fan, Wei

Published in:
I E E E Transactions on Aerospace and Electronic Systems

DOI (link to publication from Publisher):
10.1109/TAES.2022.3205289

Publication date:
2023

Document Version
Accepted author manuscript, peer reviewed version

Efficient Pre-Processing of Site-Specific Radio Channels for Virtual Drive Testing in Hardware Emulators

ALLAN WAINAINA MBUGUA
Huawei Technologies Duesseldorf GmbH, Munich Research Center, Munich, Germany and the Antennas, Propagation and Millimetre-Wave Systems (APMS) Section, Aalborg University, Aalborg, Denmark.

YUN CHEN
Huawei Technologies Duesseldorf GmbH, Munich Research Center, Munich, Germany.

LESZEK RASCHKOWSKI
Fraunhofer Institute for Telecommunications, Heinrich Hertz Institute, Berlin, Germany.

YILIN JI
Antennas, Propagation and Millimetre-Wave Systems (APMS) Section, Aalborg University, Aalborg, Denmark.

MOHAMED GHARBA
Huawei Technologies Duesseldorf GmbH, Munich Research Center, Munich, Germany.

WEI FAN, Senior Member, IEEE
Antennas, Propagation and Millimetre-Wave Systems (APMS) Section, Aalborg University, Aalborg, Denmark.

***Abstract*— Performance testing under realistic propagation channel conditions is essential for virtual drive testing (VDT), where radio channel emulators are typically employed in the laboratory for such applications. Optimal allocation of tap resources in the channel emulator is critical in hardware-in-the-loop emulation of radio channels due to the constraint of real-time operation requirements, hardware complexity and cost. As a result, replaying arbitrary site-specific e.g. measured or ray tracing (RT) simulated radio channels in channel emulators requires delay alignment and reduction in the number of multipath components (MPCs) in the channel to match the available hardware resources. However, such operations would essentially introduce inaccuracies in the emulated channel. In this paper, a framework for pre-processing site-specific radio channels for hardware emulation is proposed. The delay alignment problem is formulated as a finite impulse response (FIR) filter design problem whereas the subsequent tap reduction and selection process is formulated as a sparse approximation problem. This approach enables maximization of the accuracy of the reproduced channel frequency response (CFR) and Doppler profile in the hardware emulator using a limited number of taps. The efficiency of the proposed framework is demonstrated experimentally with a dynamic vehicular RT simulated channel which is replayed on a state-of-the-art radio channel emulator.**

***Index Terms*—Convex optimization, FIR filter, radio channel emulation, ray tracing, sparse approximation, virtual drive testing.**

Authors' addresses: A. W. Mbugua is with Huawei Technologies Duesseldorf GmbH, Munich Research Center, Munich, Germany and the Antennas, Propagation and Millimetre-Wave Systems (APMS) Section, Aalborg University, Aalborg, Denmark. (e-mail: allan.mbugua@huawei.com). Y. Chen is with Huawei Technologies Duesseldorf GmbH, Munich Research Center, Munich, Germany. (e-mail: yun.chen2@huawei.com). L. Raschkowski is with Fraunhofer Institute for Telecommunications, Heinrich Hertz Institute, Berlin, Germany. (e-mail: leszek.raschkowski@hhi.fraunhofer.de). Y. Ji is with the Antennas, Propagation and Millimetre-Wave Systems (APMS) Section, Aalborg University, Aalborg, Denmark. (e-mail: yilin@es.aau.dk). M. Gharba is with Huawei Technologies Duesseldorf GmbH, Munich Research Center, Munich, Germany. (e-mail: mohamed.gharba@huawei.com). W. Fan is with the Antennas, Propagation and Millimetre-Wave Systems (APMS) Section, Aalborg University, Aalborg, Denmark. (e-mail: wfa@es.aau.dk).

I. INTRODUCTION

TESTING wireless communication systems with realistic propagation channels is critical to ensure that optimal performance is achieved in the target deployment scenarios. Radio channel emulators enable real-time playback of arbitrary realistic radio channels in repeatable and controllable laboratory environments [1], [2]. A key benefit of fading emulators when generating arbitrary propagation channels in the lab is the ability to precisely control multipath components (MPCs) parameters such as the delay and the complex channel coefficients.

Replaying site-specific radio channels from field measurements or ray tracing (RT) simulations in the laboratory in end-to-end setups is particularly useful in virtual drive testing (VDT) for network testing and optimization [3], [4]. This is typically carried out using either conducted or over-the-air (OTA) test setups [5], [6], [7]. In both conducted and OTA test-setups, the hardware resource usage on the radio channel emulator scales up with the increase in the number of input and output radio frequency (RF) ports. The limitation of available hardware resources is thus more prevalent for massive multiple-input multiple-output (MIMO) emulation test-setups [8]. With dual-polarized antennas, each dual-polarized antenna requires two ports on the channel emulator thereby doubling the number of logical channels for a given MIMO or massive MIMO order. The constraint on hardware resources is further exacerbated in multi-user, multi-base station (BS) and multi-carrier emulation test-setups, creating a need for efficient radio channel emulator resource allocation.

State-of-the-art channel emulators used in VDT can be classified into two main categories; analog and digital emulators. In analog channel emulators, the fading environment is typically realized using programmable RF attenuators and coaxial delay lines [1]. On the other hand, digital channel emulators are typically implemented on field programmable gate arrays (FPGAs) [9], [10], [11], [12], [13], [14], which allow flexible representation of the complex channel, for example as a cluster delay

line, taped delay line, or using a subspace representation of the complex radio channel [15], [16]. Typically, the input RF signal is downconverted and the desired fading environment is generated by filtering the in-phase and quadrature (IQ) components of the baseband signal via a finite impulse response (FIR) filter [2], [1]. In most state-of-the-art commercial radio channel emulator the FIR filter tap coefficients for a given channel can be generated offline and read from the emulator's memory, i.e. filed-based emulation. This facilitates the emulation of site-specific channels, i.e. measured or RT simulated channels.

Measured and RT channels are characterized by MPCs with arbitrary delays, which need to be aligned to the sampling grid of a radio channel emulator [17]. The emulators sampling grid is usually in integer multiples of the sampling time thus the MPCs in the target site-specific channels must be approximated in this grid for emulation. To minimize the distortion of the site-specific channel frequency response (CFR) during emulation, tap alignment in theory can be carried out using an ideal fractional delay (FD) filter. In FD filters, the delay of the MPCs is decomposed into two parts, the integer and the fractional part. When the fractional part is non-zero, the ideal FD filter is non-causal with an infinite number of non-zero coefficients [18]. Therefore, the ideal FD filter cannot be used in practice.

In file-based digital radio channel emulators, various FIR filter designs can be employed to approximate the ideal FD filter for delay alignment. In [19], tap alignment is carried out by truncating the ideal FD filter with subsequent iterative path reduction until the desired number of taps is reached [20]. The phase of the remaining paths is then optimized to minimize the mean square error in the CFR. The truncation of the ideal FD yields an L_2-optimal FD FIR filter for a given order specification, but suffers from the Gibbs phenomenon [18]. In [21], delay alignment is carried out by approximating the FD with a first-order FIR filter. Although this approach is computationally efficient, low order FIR filters result in a higher magnitude and phase error in comparison to higher order FIR filters [18]. In [22], the general least squares FIR filter is used for tap delay alignment. Although this approach has been shown to achieve a good match of the CFRs, it may suffer from numerical errors when used in narrow-band applications [18]. Due to the constantly growing complexity of the scenarios to be tested, such as massive MIMO, multi-BS, and multi-user scenarios, the demand on channel emulator resources will increase significantly in the future. Using two or more synchronized emulators in a multi-emulator setup is one way to counteract this situation [23]. However, poor delay alignment strategies might not be able to exploit the available hardware resources, as demonstrated in [22]. Our work aims to address this important topic. Our contributions are as follows:

- We perform delay alignment of RT simulated channels using the minimax FIR filter, which minimizes the maximum absolute error in the magnitude of the CFR [24], [18], [25], [26]. By adding an affine constraint in the optimization objective function, the taps delay drift can be specified to match a particular hardware support. This is crucial since arbitrary drifting of tap delays across channel snapshots or antenna pairs is not possible in some emulators as outlined in [14], [27]. This delay alignment approach guarantees the preservation of the CFR and is more accurate than the conventional rounding delays or delay binning approach [3], [28].
- We demonstrate that the tap selection or reduction process of the delay aligned channel can be formulated as a sparse approximation problem. This problem is then solved using the orthogonal matching pursuit (OMP) algorithm, which ensures that each tap is selected only once [29]. The pre-processed channel is then validated using a state-of-the-art channel emulator. We illustrate that in the presence of measurement uncertainties and hardware imperfections, the main factors affecting high-fidelity playback of measured or RT simulated channels stem from the pre-processing approach employed.

The rest of the paper is organized as follows. Section II outlines the system model, Section III outlines the proposed framework, Section IV presents the ray tracing simulations and the measurement setup for validation of the emulated channel, Section V presents the results and the discussion thereof, and Section VI concludes the paper.

II. SYSTEM MODEL

In VDT, two key components are the radio channel model, which is the mathematical description of the target radio environment under which the system under test operates, and the radio channel emulator used to reproduce the radio channel in the lab. Radio channel model can be obtained from RT tools which have been shown in the literature to be sufficiently accurate cf. [30] and references therein. However, RT simulations are usually not real-time and the output format is often not readily compatible with radio emulator specifications. On the other hand, radio channel emulators and in particular commercially available emulators are designed for real-time and have a fixed amount of hardware resources. Therefore, radio channels generated using RT tools need to be pre-processed to meet the specification of a given radio channel emulator. In this Section, the mathematical description of radio channels from RT is outlined as well as the target hardware structure for the proposed pre-processing framework.

A. Channel Model

Consider a MIMO system with U BS and S mobile terminal (MT) antennas, respectively. Given that the channel is composed of M MPCs, the time variant CFR between the BS antenna $u \in [1, U]$ and MT antenna $s \in [1, S]$ can be expressed as:

$$H_{u,s}(t,f) = \sum_{m=1}^{M} \begin{bmatrix} G_s^{\mathrm{V}}(\mathbf{\Omega}_{\mathrm{Rx}}, f) \\ G_s^{\mathrm{H}}(\mathbf{\Omega}_{\mathrm{Rx}}, f) \end{bmatrix}^T \begin{bmatrix} \alpha_m^{\mathrm{VV}}(t,f) & \alpha_m^{\mathrm{VH}}(t,f) \\ \alpha_m^{\mathrm{HV}}(t,f) & \alpha_m^{\mathrm{HH}}(t,f) \end{bmatrix} \begin{bmatrix} G_u^{\mathrm{V}}(\mathbf{\Omega}_{\mathrm{Tx}}, f) \\ G_u^{\mathrm{H}}(\mathbf{\Omega}_{\mathrm{Tx}}, f) \end{bmatrix} \cdot \exp\left(-j2\pi f \tau_m\right) \tag{1}$$

where f is the frequency, τ_m is the delay of the m-th MPC, α_m^{VV}, α_m^{HH}, α_m^{VH} and α_m^{HV} are the vertical co-polar, horizontal co-polar, vertical cross-polar and horizontal cross-polar components for the m-th path, respectively. G^{V} and G^{H} are the complex antenna radiation pattern components for the vertical and horizontal polarization for the BS or MT antenna, respectively. $\mathbf{\Omega}_{\mathrm{Rx}} = [\theta, \phi]$ and $\mathbf{\Omega}_{\mathrm{Tx}} = [\theta, \phi]$ are the angle of arrival and departure, respectively, where θ and ϕ are the elevation and azimuth angles, respectively.

In radio channel emulation, depending on the mobile speed under consideration, a time series of R channel impulse responses (CIRs) is required. The update rate of the CIRs f_{upd} can be determined based on the fading resolution required as follows [31], [32]:

$$f_{\mathrm{upd}} = 2 \cdot \mathrm{SD} \cdot \nu_{\mathrm{max}} \tag{2}$$

where the sample density SD, is the number of CIRs per half wavelength and ν_{max} is the maximum Doppler frequency.

B. Hardware Structure

Fig. 1 shows a block diagram of a generic digital channel emulator comprising U tap units, S logical channels per tap unit, and support for a $U \times S$ MIMO configuration. The input and output ports in digital fading emulators are connected in a mesh structure, with each logical channel representing the channel between the different transmitter (Tx) and receiver (Rx) antenna pairs [2], [1]. Each logical channel is implemented as an FIR filter, where each tap of the FIR filter is realized using hardware multipliers [1]. For a given channel emulator the number of hardware multipliers is limited and fixed. Therefore, to accommodate higher-order MIMO, the hardware multipliers allocated to each logical channel are reduced and consequently the number of taps available for each logical channel are reduced as well.

The tap units are typically implemented on FPGAs, where each tap $q \in [1, Q]$ is realized using hardware multipliers, for example 4 in [1]. In higher-order MIMO emulation, different pairs of Tx and Rx antennas are multiplexed to utilize the same tap unit, resulting in a lower number of taps per logical channel [2]. Typically, the maximum number of taps available per logical channel in state-of-the-art channel emulators are 48 in [23], 24 in [33], and 20 in [2].

III. Proposed Framework

In VDT, one key goal is to reproduce (1) as accurately as possible in the laboratory. File-based digital radio channel emulators are often implemented using FIR filters [27]. Similarly, radio channels can be modeled as FIR filters with an arbitrary magnitude and phase response. Based on this observation the proposed framework of pre-processing site-specific radio channels for replay in file-based digital channel emulators is thus composed of two stages: a) tap delay alignment which is essentially an FIR filter design problem and b) tap selection process for the delay aligned channel which is posed as a sparse approximation problem.

A. Tap Delay Alignment

As mentioned in Section I, in practice the delays of the M MPCs in (1) are not guaranteed to be at the sampling instance of a given radio channel emulator. For a given channel emulator with a sampling frequency F_s, the delays of the m-th MPC in (1) can be expressed in samples as:

$$D_m = \tau_m F_s \tag{3}$$

The delay alignment of these MPCs is basically a band-limited interpolation problem that can be solved using a FD filter [18]. In a FD filter, the non-integer part of the delay in samples D, is approximated by interpolating the tap coefficient in the N sampling instances. This is in contrast to rounding delays where the non-integer delay in samples D, is approximated to the nearest sampling interval on the sampling grid [28]. For an ideal FD FIR filter, the non-zero tap coefficients span over an infinite number of sampling instances and is non-causal. The resulting frequency response can thus be expressed as:

$$\bar{H}_{u,s}(t,\omega) = \sum_{n=-\infty}^{\infty} c_{u,s}[n](t) \exp(-j\omega n) \tag{4}$$

where $\bar{H}_{u,s}(t,\omega)$ is the frequency response of the ideal fractional delay filter for the u,s-th BS-MT link at the normalized frequency $\omega \in [0, 2\pi]$, and $c_{u,s}[n](t)$ contains the tap coefficient for the sampling instance $n \in [-\infty, \infty]$. The normalized frequency ω is denoted as:

$$\omega = \frac{2\pi f}{F_s} \tag{5}$$

The ideal FD filter as shown in (4), is not realizable in practice. FIR filters, are thus used to approximate the ideal FD filter in hardware limited regimes, where for an N length FIR filter, the frequency response can be expressed as:

$$\hat{H}_{u,s}(t,\omega) = \sum_{n=0}^{N-1} c_{u,s}[n] \exp(-j\omega n). \tag{6}$$

$c_{u,s}[n]$ contains the tap coefficient for the sampling instance $n \in [0, N-1]$. The accuracy of the reproduced CFR $\hat{H}_{u,s}(t,\omega)$ using an FIR filter, is determined by several factors e.g. the type of FIR filter, the filter length, the

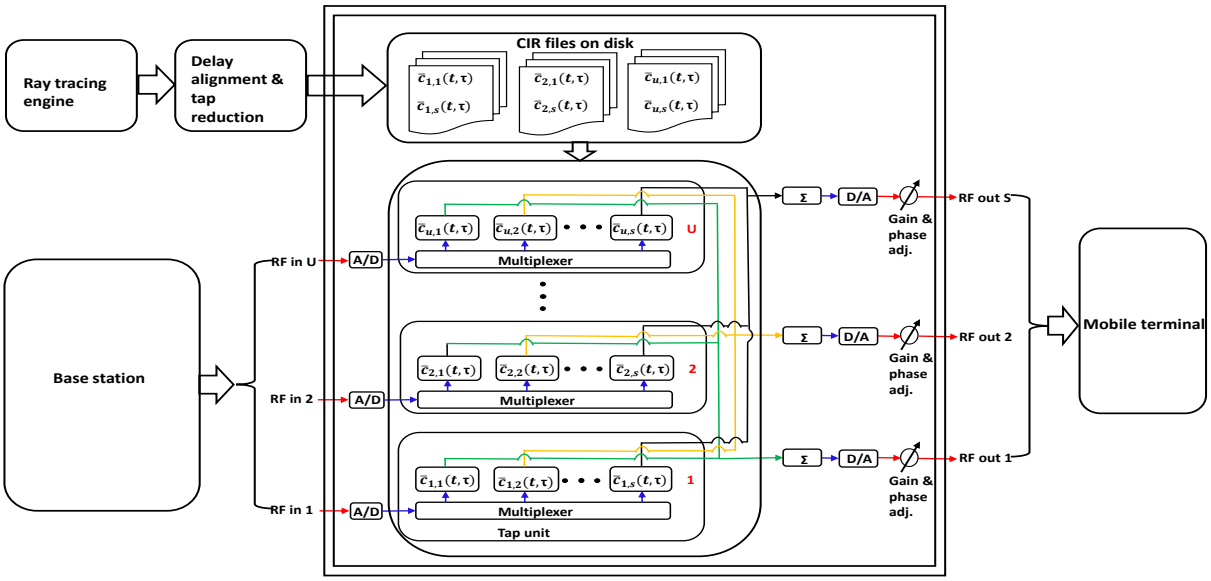

Fig. 1. Block diagram of a typical digital radio channel emulator. A/D and D/A denotes analog to digital and digital to analog conversion, respectively.

relative location of the delay with respect to the filter length and the FD value [18], [34]. Besides the FD value, which is determined by the absolute delay of the MPCs in measured or RT simulated channels, it is crucial to carefully select the filter type and its length.

1. FIR Filter Realization

The minimax FIR filter design to approximate a desired FD filter ensures that for a given filter specification the maximum absolute error of the CFR is minimized. To determine the filter coefficients, we use CVX, a package for specifying and solving convex programs [35], [36], with the following objective function:

$$\min \max_{\omega\in[0,2\pi]} \quad |\hat{H}_{u,s}(t,\omega) - H_{u,s}(t,\omega)| \tag{7}$$

where $H_{u,s}(t,\omega)$ is the target frequency response in (1) and $|\cdot|$ denote the absolute value. The target frequency response $\mathbf{h}_{u,s}(t) \in \mathbb{C}^{L\times 1}$ for L frequencies can be defined as:

$$\mathbf{h}_{u,s}(t) = \begin{bmatrix} H_{u,s}(t,\omega_1) & H_{u,s}(t,\omega_2) & \cdots & H_{u,s}(t,\omega_L) \end{bmatrix}^T. \tag{8}$$

Therefore, (7) can be reformulated as [34]:

$$\min_{\mathbf{c}_{u,s}(t)} \max \quad |\mathbf{A}\mathbf{c}_{u,s}(t) - \mathbf{h}_{u,s}(t)| \tag{9}$$

where $\mathbf{A} \in \mathbb{C}^{L\times N}$ is a full rank Vandermonde matrix defined as follows:

$$\mathbf{A} = \begin{bmatrix} \mathbf{a}_0 & \cdots & \mathbf{a}_{N-1} \end{bmatrix} \tag{10}$$

with $L \gg N$. The entries in (10) are defined as follows:

$$\mathbf{a}_n = \begin{bmatrix} \exp(-jn\omega_1) & \exp(-jn\omega_2) & \cdots & \exp(-jn\omega_L) \end{bmatrix}^T. \tag{11}$$

The vector $\mathbf{c}_{u,s}(t) \in \mathbb{C}^{N\times 1}$ contains the delay aligned coefficients obtained with the minimax FIR filter for a given target channel, where N is the filter length. For the specified frequency range, the coefficients obtained with the minimax FIR filter are guaranteed to minimize the maximum error in the magnitude of the CFR. An additional intuitive benefit of using the minimax FIR filter is that channel measurement data collected in the frequency domain, for example with a vector network analyzer (VNA), can be processed for playback in the channel emulator without the need to perform parameter estimation. As outlined in [14], different radio channel emulators have different ways to implement delay drift (the temporal evolution of an MPC) depending on the hardware complexity. The formulation in (9) allows for flexible adaptation of the delay alignment per channel snapshot to the hardware capabilities of a particular channel emulator. For example, drifting delays can be supported by adding an affine constraint to the objective function as follows:

$$\begin{aligned} \min_{\mathbf{c}_{u,s}(t)} \max \quad & |\mathbf{A}\mathbf{c}_{u,s}(t) - \mathbf{h}_{u,s}(t)| \\ \text{s.t.} \quad & c_{u,s}[n](t) = 0, \ n \in \boldsymbol{\Xi} \end{aligned} \tag{12}$$

where the vector $\boldsymbol{\Xi}$ contains the deactivated tap indices. Although this formulation allows for support of different hardware architectures, the penalty is a reduction in the accuracy of the delay aligned CFR.

2. FIR Filter Length Selection

The minimax FIR filter (9) or (12), is solved for each (u,s)-th BS-MT link and at each time snapshot. Since the delays of the MPCs are different in each channel snapshot, it is not prudent to fix the FIR length N. This is because the degrees of freedom of the optimization in (9) or (12), depend on the number of FIR coefficients which can be at most N. A small number of FIR coefficients result in the reduction of the degrees of freedom available and hence a reduction in the achieved accuracy. The filter length N of the minimax FIR filter is thus a crucial parameter as it determines the resulting accuracy in terms

of minimizing the maximum absolute error of the CFR. However, using an excessively long filter will result in increased computation with marginal gain in the accuracy. On the other hand, using a short filter length will result in a reduction of the accuracy of the achieved solution.

To ensure that the optimal solution is obtained, the FIR filter length N is computed for each channel snapshot in each of the (u, s)-th BS-MT links. This is computed as the maximum delay of the dominant paths that contain a certain power threshold. In this paper, unless otherwise stated, a threshold of 99.999% is chosen.

B. Tap Selection

The solution of (9) or (12), i.e. the vector $\mathbf{c}_{u,s}(t) \in \mathbb{C}^{N\times 1}$, may contain up to N non-zero coefficients, which may be much greater than the number of tap coefficients supported in most radio channel emulators. Tap selection is thus necessary to reduce the number of non-zero tap coefficients to at most Q. The tap selection process can then be carried out using OMP [29] based on the following observations:

- The significant part of the energy of the band-limited interpolated taps (delay aligned taps) in the vector $\mathbf{c}_{u,s}(t) \in \mathbb{C}^{N\times 1}$ are located in the delay bins closest to the delay of the MPCs in the target CIR.
- The number of dominant taps in $\mathbf{c}_{u,s}(t) \in \mathbb{C}^{N\times 1}$, i.e. taps containing most of the channel power, is much smaller compared to the total number of taps N. This is illustrated in Fig. 2 for the RT simulated channel outlined in Section IV. In this case it can be observed that in approximately 92% of channel snapshots analyzed, 99% of the total channel power is contained within 20%, 28.2%, and 38.5% of the delay aligned taps for the urban macro, campus, and indoor scenarios, respectively. This indicates sparsity in the delay domain τ, thus enabling the formulation of the tap selection process as a sparse approximation problem.

Let the CFR $\hat{\mathbf{h}}_{u,s}(t)$ with delay aligned taps be defined as:

$$\hat{\mathbf{h}}_{u,s}(t) = \begin{bmatrix}\hat{H}_{u,s}(t,\omega_1) & \hat{H}_{u,s}(t,\omega_2) & \cdots & \hat{H}_{u,s}(t,\omega_L)\end{bmatrix}^T \tag{13}$$

then the tap selection procedure is performed iteratively until the desired number of taps Q is attained as follows.

- Step 1: The residual vector is initialized as $\mathbf{r}_0(t) = \hat{\mathbf{h}}_{u,s}(t)$, the iteration counter $i = 1$ and the matrix $\mathbf{B} \in \mathbb{C}^{L\times N} = \mathbf{0}$.
- Step 2: The tap index q at the i-th iteration is found as the column of (10) with the highest correlation with the residual vector

$$q_i(t) = \arg\max |\mathbf{A}^H \mathbf{r}_{i-1}(t)| \tag{14}$$

  where $(\cdot)^H$ is the Hermitian transpose.
- Step 3: Update the q-th column of the matrix $\mathbf{B}$ as $\mathbf{b}_q = \mathbf{a}_q$ and set the column of (10) corresponding to the selected tap as $\mathbf{a}_q = \mathbf{0}$.

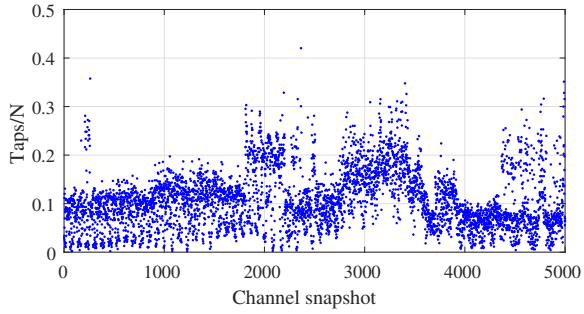

(a)

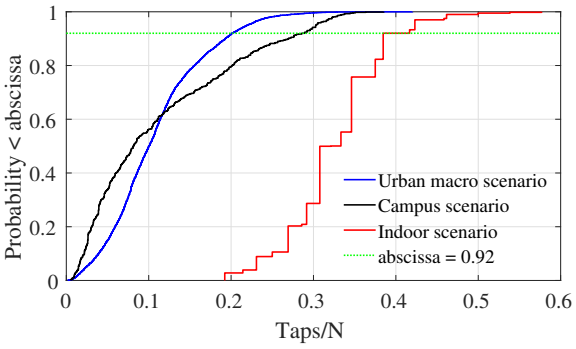

(b)

Fig. 2. (a) Ratio of the number of taps with 99% of the total channel power to the filter length per channel snapshot for the urban macro scenario. (b) Empirical cumulative distribution function of the ratio of the number of taps with 99% of the total channel power to the FIR filter length for the urban macro, campus and indoor scenarios.

- Step 4: The tap coefficient minimizing the least square error can then be obtained as:

$$\min_{\bar{\mathbf{c}}^i_{u,s}(t)} ||\mathbf{B}\bar{\mathbf{c}}^i_{u,s}(t) - \hat{\mathbf{h}}_{u,s}(t)||_2^2 \tag{15}$$

  where $||\cdot||_2$ is the L_2 norm.
- Step 5: Update the residual as

$$\mathbf{r}_i(t) = \hat{\mathbf{h}}_{u,s}(t) - \mathbf{B}\bar{\mathbf{c}}^i_{u,s}(t). \tag{16}$$

- Step 6: Update the iteration counter i and repeat step 2 through step 5 until the number of taps selected equals the target number of taps Q.

Finally, the delay aligned CFR with tap selection can be obtained as:

$$\bar{\mathbf{h}}_{u,s}(t) = \begin{bmatrix}\bar{H}_{u,s}(t,\omega_1) & \bar{H}_{u,s}(t,\omega_2) & \cdots & \bar{H}_{u,s}(t,\omega_L)\end{bmatrix}^T \tag{17}$$

where

$$\bar{H}_{u,s}(t,\omega) = \sum_{i=1}^{Q} \bar{c}_{u,s}[q_i](t)\exp(-j\omega q_i). \tag{18}$$

IV. RAY TRACING SIMULATIONS AND RADIO EMULATOR MEASUREMENT SETUP

The validation of the proposed framework is carried out using three representative scenarios i.e. an urban macrocell (UMa), a campus, and an indoor scenario. The

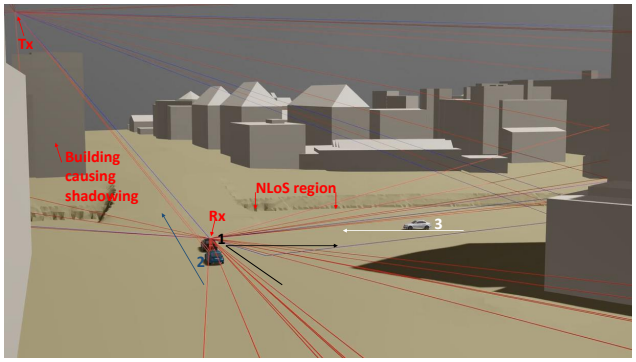

Fig. 3. An illustration of the RT simulated vehicular scenario and selected dominant MPCs. Reflected paths are shown in blue and diffracted paths in orange. The arrows indicate the trajectories of each car.

CFRs of the time variant channels i.e. (1) are then pre-processed with the proposed framework i.e. tap delay alignment and tap selection. The tap coefficients of the the pre-processed UMa scenario, $\bar{\mathbf{c}}_{1,1}(t)$ and their corresponding delays are then replayed on a state-of-the-art radio channel emulator to demonstrate the efficiency of the proposed framework.

A. Ray Tracing Simulations

1. *Urban Macro Scenario*

An RT simulation in an UMa scenario in Berlin with three moving vehicles is considered to mimic a drive test along a track length of 100 m. The Tx is placed at a height of 42.5 m on top of a building and the Rx is placed at a height 1.5 m on car #1 as illustrated in Fig. 3. Car #1 drives on a straight course towards the Tx and takes a right turn at the street intersection. CIRs are generated according to the update rate in (2) at an average speed of 1 m/s at a frequency of 2.6 GHz, resulting in 5000 CIRs. The channel is dominated by the line-of-sight (LoS) path except at channel snapshots 2735 to 4367 corresponding to the region near the street intersection where there is shadowing from the building next to the Tx. Due to the complexity of the simulation, the interaction mechanisms are limited to diffraction and reflection only with a maximum order of 1 and 6, respectively. Diffraction is modeled using the uniform theory of diffraction (UTD) [37], while reflections are evaluated using Fresnel's reflection coefficients. In the simulation, the Tx and Rx antennas are vertically polarized with an omni-directional radiation pattern in the azimuth and a gain of 0 dBi.

Note that the raytracer was validated using measurement campaigns conducted at the same site. Details of the measurement data used for validation are outlined in [38]. As this work focuses on the pre-processing of the raytracer's output for playback in a hardware channel emulator and not on the raytracer itself, the results of its validation are not included here.

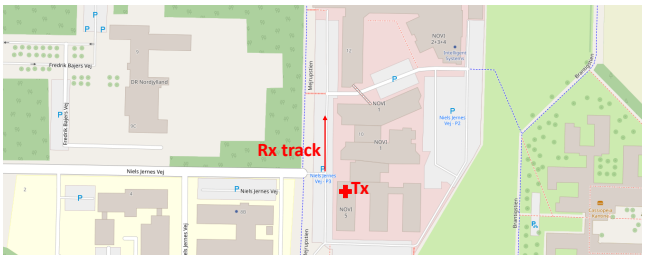

Fig. 4. An illustration of the Aalborg University campus scenario from Open Street Maps.

Fig. 5. An illustration of the indoor scenario [39].

2. *Campus Scenario*

A 28.8 m track is considered in the Aalborg University campus. Since there are no moving objects in the scenario the channel is sampled spatially at intervals of 0.0288 m to generate 1001 channel snapshots. The BS and MT antennas at a height of 22.5 m and 1.5 m, respectively as illustrated in Fig. 4.

3. *Indoor Scenario*

An indoor scenario i.e. a classroom is considered as shown in Fig. 5 [39]. The dimensions of the scenario are $10.2 \times 8.5 \times 3.1$ m. Similar to the campus scenario, no moving objects are present in the scenario hence the channel is sampled spatially along a track of 3.6 m at intervals of 0.0036 m to generate 1001 channel snapshots. The BS and MT antennas are both placed at a height of 1 m.

B. Measurement Setup

The validation of the emulated channel is carried out for a single-input single-output (SISO) setup using a VNA as shown in Fig. 6. In a SISO setup a maximum of 48 taps are available in the radio channel emulator, however, the number of taps is set as $Q = 12$ in the pre-processing to mimic a limited number of taps as would be the case in a massive MIMO setup. We have selected $Q = 12$ as a typical value which can be achieved in a massive MIMO setup e.g. on a state-of-the-art emulator cf. [23] based on the authors' experience. However, this should not be interpreted as the upper limit for the massive MIMO case.

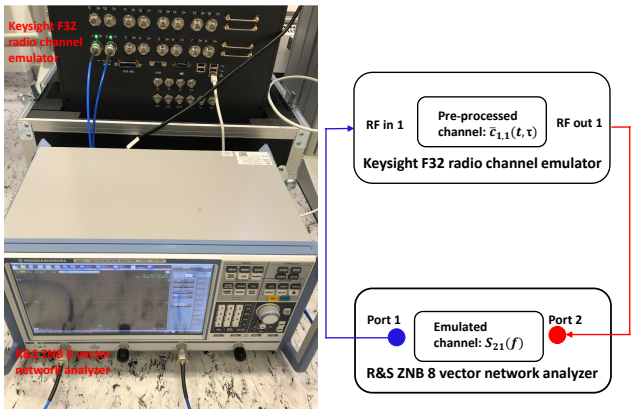

(a) (b)

Fig. 6. (a) A photo of the measurement setup for validation of the emulated CFR. (b) A block diagram of the measurement setup.

TABLE I
Measurement equipment and parameters.

Equipment/Parameter	Value
Channel emulator	Keysight F32
Emulator sampling clock frequency	200 MHz
Emulator bandwidth	40 MHz
VNA	R&S ZNB 8
Frequency	2.6 GHz
VNA intermediate frequency bandwidth	500 Hz
VNA bandwidth	40 MHz
Number of frequency points	1001
VNA port 1 power	0 dBm

The pre-processed taps coefficients $\bar{\mathbf{c}}_{1,1}(t)$ of the RT simulated channel and their respective delays obtained in Section III-B are loaded and replayed on the radio emulator in step mode, i.e. the emulator is paused after the replay of each channel snapshot. This ensures that the VNA completes the frequency sweep for the current snapshot before measuring the next CFR. The CFR for each snapshot is thus recorded as the S-parameter $S_{21}(f)$ on the VNA. The bandwidth of the VNA was set to 40 MHz according to the available bandwidth of the channel emulator as shown in Table I. Although the emulator sampling rate is 200 MHz, the sampling grid of the specific device used herein was shipped with a sampling grid fixed to 20 ns and not 5 ns.

V. RESULTS AND DISCUSSION

In the pre-processing results, a bandwidth of 100 MHz is considered which is the maximum alias free bandwidth for the considered sampling rate of 200 MHz. This is in order to illustrate the applicability of the proposed framework to wideband channels. However, the radio channel emulator used in the measurement setup has a bandwidth of 40 MHz and thus the difference in the considered bandwidth for the simulated and emulated channels.

A. Evaluation metrics: Definition

1. *Frequency Response Assurance Criterion*

The frequency response assurance criterion (FRAC) [40], [41] is a commonly used measure in modal analysis for comparing the shape for two frequency responses functions for linear time invariant systems. For radio emulation, we desire to preserve the target CFR after delay alignment and tap selection to ensure that indeed the measured or RT simulated channel is replayed on the fading emulator. The FRAC gives a quantitative similarity metric between two CFR and can be expressed as:

$$\rho(t) = \frac{|\bar{\mathbf{h}}_{u,s}^H(t)\mathbf{h}_{u,s}(t)|^2}{(\bar{\mathbf{h}}_{u,s}^H(t)\bar{\mathbf{h}}(t))(\mathbf{h}_{u,s}^H(t)\mathbf{h}_{u,s}(t))} \tag{19}$$

with $\rho(t) \in [0,1]$ where $\rho(t) = 1$ indicates a high correlation between the target CFR and the CFR obtained after delay alignment and tap selection.

2. *Magnitude Error*

The accuracy of the delay aligned and tap reduced CFR can be evaluated by considering the magnitude error of the reproduced CFR. The deviation in the magnitude $\mathbf{\Delta}\alpha$ is computed using the equivalent stray signal (ESS) [42], [43] that is commonly used in antenna measurements for comparing the antenna gain pattern when the measurement is performed under slightly different conditions. A low value of the ESS indicates a good match in the result. The ESS ($\mathbf{\Delta}\alpha$) is expressed as:

$$\mathbf{\Delta}\alpha(t) = \zeta(t) + 20\log_{10}\left(\frac{1-10^{-\epsilon(t)/20}}{2}\right) \tag{20a}$$

$$\zeta(t) = |\max(\xi(t), \bar{\xi}(t))| \tag{20b}$$

$$\epsilon(t) = |\xi(t) - \bar{\xi}(t)| \tag{20c}$$

$$\xi(t) = 20\log_{10}(|\mathbf{h}_{u,s}(t)|) - \max(20\log_{10}(|\mathbf{h}_{u,s}(t)|)) \tag{20d}$$

$$\bar{\xi}(t) = 20\log_{10}(|\bar{\mathbf{h}}_{u,s}(t)|) - \max(20\log_{10}(|\bar{\mathbf{h}}_{u,s}(t)|)) \tag{20e}$$

B. Pre-Processed Simulated Channels

1. *Frequency Response Assurance Criterion*

In the UMa scenario, where the channel is dominated by the LoS component from channel snapshot 1 to 2734, the FRAC value for the rounding delays method can be seen to increase and decrease periodically as illustrated in Fig. 7(a). This is because the FD of the LoS component progressively changes from 0 to 0.5 as car #1 moves in the scene. As the FD approaches 0.5, the CFR phase error increases resulting in a lower FRAC value. When the FD is close to 0 the FRAC value with rounding delays approaches 1 due to a reduction in the CFR phase error. In the non-line-of-sight (NLoS) regions, channel snapshot 2735 to 4367, the impact of the FD value of different

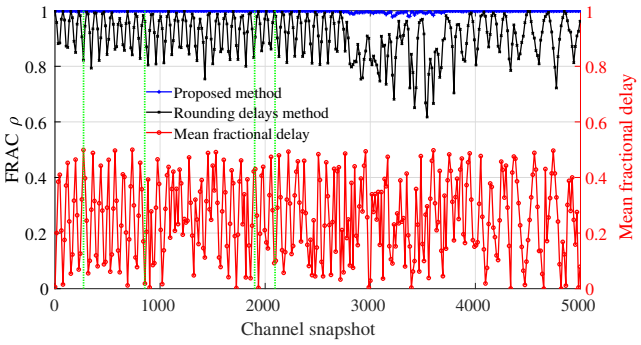

(a)

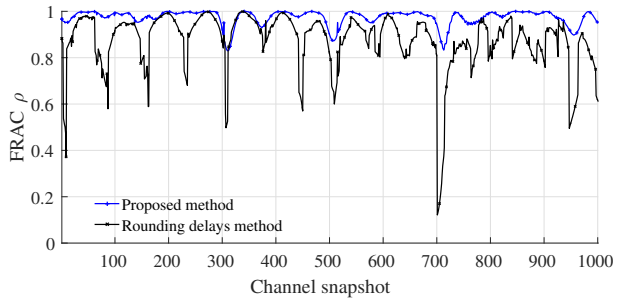

(b)

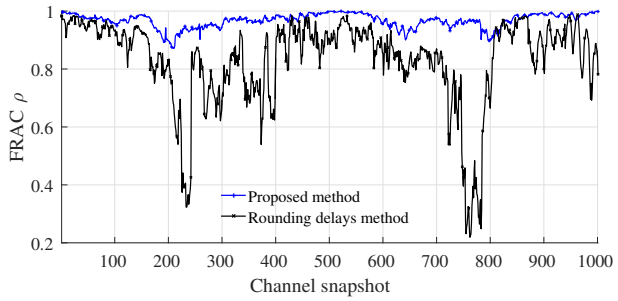

(c)

Fig. 7. A comparison of the FRAC of the pre-processed complex CFR for the the proposed method and rounding delays method with 12 taps, 5 ns tap spacing, and 100 MHz bandwidth. (a) UMa scenario where the mean FD in the RT simulated channel is also shown to highlight the dependence of the accuracy of the rounding delays method on the fractional delay of the MPCs. (b) Campus scenario. (c) Indoor scenario.

MPCs becomes more pronounced due to a reduction in the relative power difference. This is reflected in a reduction in the FRAC value.

The proposed approach can be observed to be robust in the preservation of the CFR due to an excellent preservation of the channel phase. To further illustrate this, we consider the mean FD for all snapshots which is evaluated as follows.

$$\mathrm{FD}_\mu = \begin{cases} 1-(\tau_\mu - \lfloor \tau_\mu \rfloor), & \text{if } \tau_\mu - \lfloor \tau_\mu \rfloor > 0.5. \\ \tau_\mu - \lfloor \tau_\mu \rfloor, & \text{otherwise.} \end{cases} \tag{21}$$

where τ_μ is the mean delay in samples for each channel snapshot, which is given as

$$\tau_\mu = F_s \frac{\sum_{m=1}^{M} |\eta_m|^2 \tau_m}{\sum_{m=1}^{M} |\eta_m|^2} \tag{22}$$

where η_m is the amplitude of the m-th MPC. Fig. 7(a) clearly shows that for the rounding delays approach the FRAC value is highly dependent on the FD. With the proposed approach the phase of the channel is more robust to the constantly changing FDs, allowing for a more natural evolution of the channel during emulation. This is even more critical in the millimeter-wave (mm-wave) frequency bands since in most hardware channel emulators the sampling clock frequency is fixed, implying that the phase error would be significantly higher with the rounding delay approach.

In the campus and indoor scenarios, the proposed framework results in a high fidelity reproduction of the channel as illustrated in Fig. 7(b) and Fig. 7(c), respectively. In both scenarios and in all the channel snapshots, the proposed framework attains a FRAC greater than 0.8. This is in contrast to the rounding delays method which exhibits an erratic performance especially for the indoor scenario.

2. *Magnitude Error*

The calculated ESS values over frequency and snapshot dimension are shown in Fig. 8 for a bandwidth of 100 MHz. As illustrated in Fig. 8(a), in the proposed approach the magnitude deviation across frequency and channel snapshots is consistent even for channel snapshots in the NLoS regions. On the other hand, for the conventional approach of rounding delays to the nearest delay bin and selecting the dominant taps, the magnitude deviation is erratic across frequency and channel snapshots as shown in Fig. 8(b). On average across frequency and channel snapshots, the proposed framework achieves a magnitude deviation of -39.8 dB, -33.5 dB, and -29.7 dB for the UMa, campus, and indoor scenarios, respectively. In comparison, the rounding delays method achieves a magnitude deviation of -30.7 dB, -25.5 dB, and -22.8 dB for the UMa, campus, and indoor scenarios, respectively.

The mean deviation of the magnitude of the CFR across frequency for the three scenarios is illustrated in Fig. 9. In most of the channel snapshots considered, the proposed method outperforms the rounding delays method. Indeed, in some channel snapshots the performance difference is as much as 20 dB. For the three scenarios considered, the indoor scenario is the most challenging for the proposed approach as illustrated in Fig. 9(c). This is because for indoor scenarios, a shorter FIR filter length N is obtained due to the shorter delays of the MPCs in such scenarios compared to campus and UMa scenarios. Consequently, the degrees of freedom for the optimization in (9) or (12) are reduced and hence a reduced accuracy. Nonetheless, the proposed method outperforms the rounding delays approach in such challenging scenarios.

C. Emulated Pre-Processed Channel

In the emulation, only the UMa scenario is considered. This is because the radio channel emulator replays the

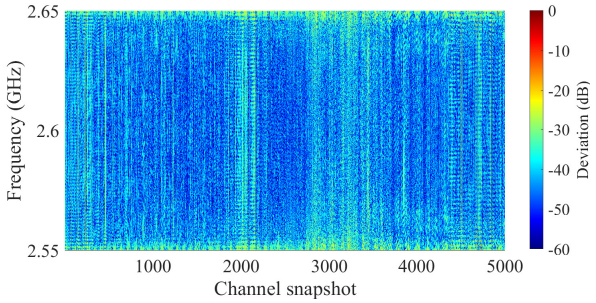

(a)

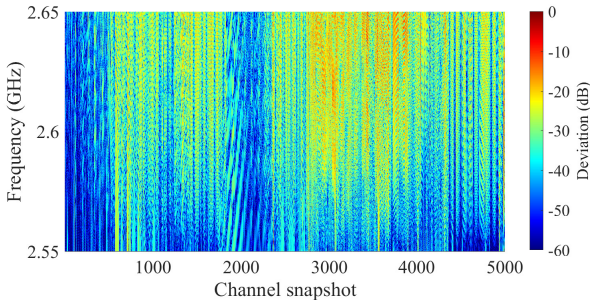

(b)

Fig. 8. Magnitude deviation computed using the ESS for 100 MHz bandwidth with 12 taps and 5 ns tap spacing for the UMa scenario. (a) Proposed method (b) rounding delays method.

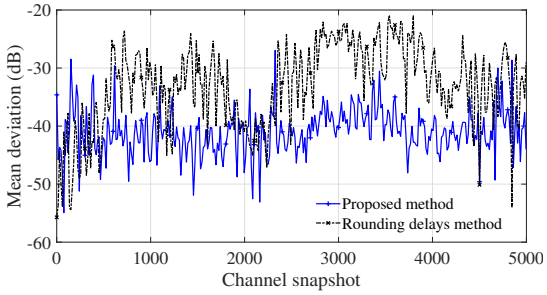

(a)

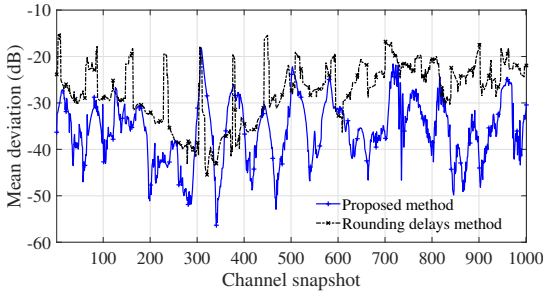

(b)

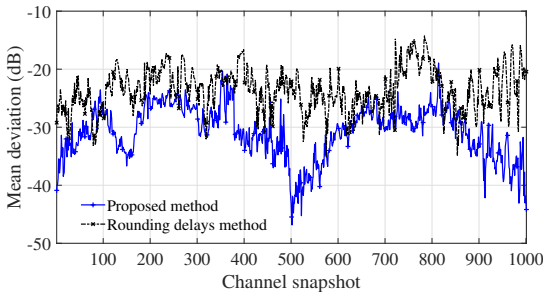

(c)

Fig. 9. Mean magnitude deviation computed using the ESS for 100 MHz bandwidth with 12 taps and 5 ns tap spacing. (a) UMa scenario. (b) Campus scenario. (c) Indoor scenario.

loaded pre-processed channel with high fidelity hence it is expected that a similar performance would be obtained for the campus and indoor scenarios.

The CIR and CFR of an exemplary emulated channel snapshot are shown in Fig. 10 for a bandwidth of 40 MHz. The emulated CIR is observed to match well with the pre-processed CIR as shown in Fig. 10(a). The discrete paths from the RT simulation denoted here as RT simulated paths are highlighted for comparison with the discrete pre-processed taps loaded in the emulator. Since the measured emulated channel is band limited i.e. 40 MHz, the RT simulated channel is band-limited as well to 40 MHz, denoted here as RT simulated CIR for comparison purposes. The RT band-limited can be seen to contain more peaks than the pre-processed and the emulated CIRs. This is because all the simulated paths are considered while in the pre-processed CIR and consequently in the emulated CIR only 12 paths are considered. Although the tap spacing on the emulator is 20 ns while the minimum delay resolution with a 40 MHz bandwidth is 25 ns, the scope of this work is the evaluation of the emulated CFR and not an estimation of the discrete emulated paths from the measured CFR hence this difference is not expected to affect the selected evaluation metrics.

The emulated CFR matches quite well to the pre-processed and RT simulated channels. The observed differences in the gain could be due to a combination of several factors: a) the non-ideal coaxial cables used in the measurement setup, b) the RF output accuracy of the channel emulator that is specified within $< \pm 0.5$ dB, c) the measurement uncertainty of the VNA, d) drift from the calibration reference of either the VNA or the channel emulator, and e) the tap spacing in the emulator is set to 20 ns while in the pre-processing it was set to 5 ns.

The accuracy of the emulated channel shown in Fig. 10 can be improved by increasing the number of taps Q. The highest accuracy obtainable is with $Q = N$. If N is greater than the maximum taps supported by a given radio channel emulator, the limiting factor on the accuracy is the number of taps supported on the emulator. However, in some cases for example channels with few dominant MPCs increasing the number of taps beyond Q would result in a marginal increase in the accuracy if the total contribution of the remaining $Q - N$ taps is minimal.

It is worthwhile to highlight here that the tap spacing constraint on the channel emulator is the main factor that contributed most to the observed deviations in Fig. 10. This is because the tap delays are automatically rounded in the emulator to the nearest sampling interval on a grid with a tap spacing of 20 ns. Nonetheless, in radio emulators where a tap spacing of 5 ns is possible, for example [23], it is expected that the emulated CFR would match

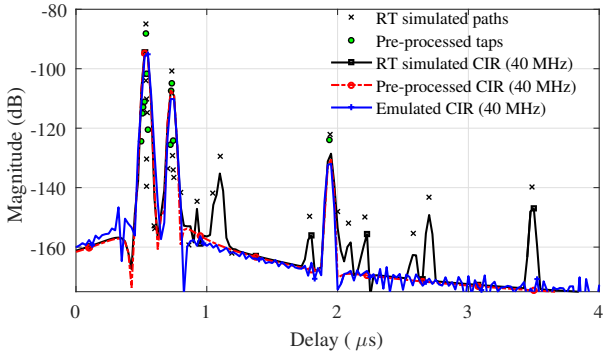

(a)

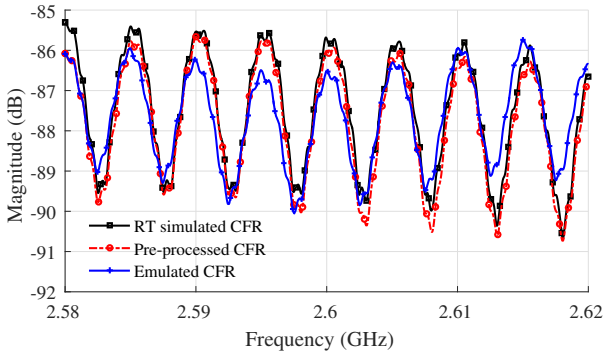

(b)

Fig. 10. A comparison of the exemplary emulated channel with 12 taps and 20 ns tap spacing to the RT simulated channel and the pre-proposed channel with 5 ns tap spacing. (a) CIR obtained with a Kaiser window with $\beta = 6$. (b) CFR.

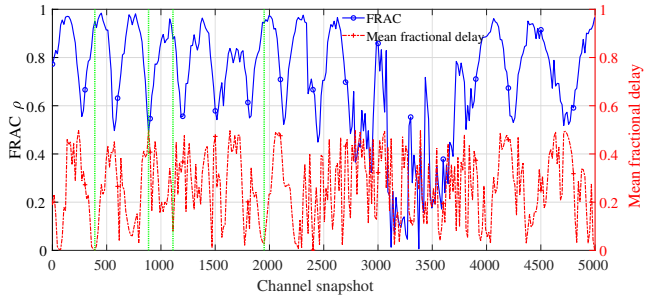

Fig. 11. FRAC of the emulated UMa channel with 20 ns tap spacing in comparison to the pre-processed complex CFR with 5 ns tap spacing for a 40 MHz bandwidth. The mean FD in the RT pre-processed channel for a 20 ns tap spacing. The dashed vertical lines highlights corresponding channel snapshots highlighted in Fig. 12.

the pre-processed CFR with the proposed approach as outlined in Section V-B, where possible minor deviations could still occur due to factors a) to d). To illustrate this, we consider the mean FD (21) of the pre-processed channel assuming a tap spacing of 20 ns. When the mean FD is close to zero, it implies lower phase errors will occur in the emulated channel. This can be observed in the FRAC value, which is shown in Fig. 11. It can be seen that the FRAC value varies greatly with the phase error due to a change in tap spacing, especially for the LoS dominated channel snapshots. This is similar to the observation made for the rounding delays approach in Fig. 7(a).

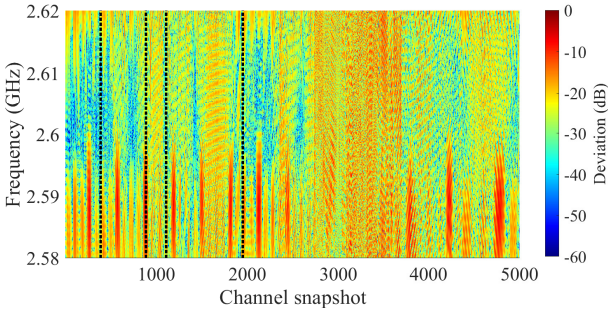

(a)

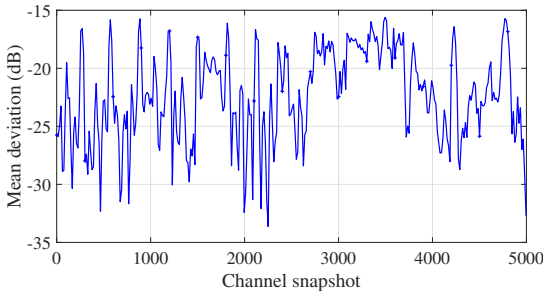

(b)

Fig. 12. Magnitude deviation of the emulated channel with 20 ns tap spacing in comparison with the pre-processed channel with 5 ns tap spacing. (a) The deviation across frequency and channel snapshots where the dashed vertical lines highlights corresponding channel snapshots highlighted in Fig.11. (b) Mean magnitude deviation across frequency for each channel snapshot.

Phase errors due to the difference in tap spacing between the pre-processed channel and emulator setting cause the peak and nulls of the CFR to shift. This can be observed in Fig. 12(a), where channel snapshots with a mean FD close to zero in Fig. 11 have a corresponding lower magnitude deviation compared to channel snapshots with a mean FD close to 0.5. The average deviation across frequency can be observed in Fig. 12(a), where the mean deviation across all frequencies and channel snapshots is -21.5 dB.

The Doppler profiles for the RT simulated channel, pre-processed channel with the proposed approach, pre-processed channel with the rounding delays approach and the emulated channel are illustrated in Fig. 13. The similarity of the pre-processed and emulated channels' Doppler profiles to the RT simulated channel Doppler profile, can be computed on the Doppler frequency components for each time instance using the FRAC. The proposed approach results in a robust preservation of the Doppler profile with a mean FRAC of 0.99 in all time instances compared to the rounding delays approach with a mean FRAC of 0.83 and 0.77 in the LoS and NLoS time instances, respectively, as illustrated in Fig. 14. This further highlights the importance of preservation of the amplitude and phase of individual channel snapshots for high fidelity fading emulation.

Due to the 20 ns tap spacing setting in the emulator, the similarity of the Doppler profile of the emulated channel to the RT simulated channel is reduced with

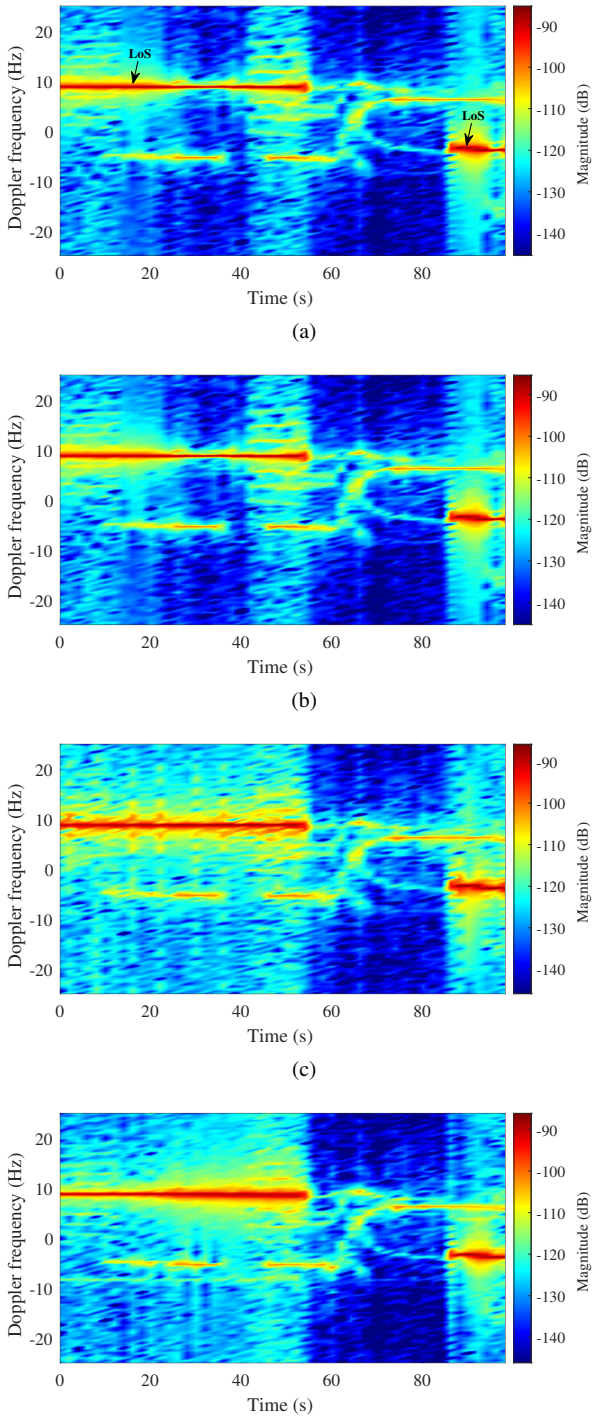

Fig. 13. Doppler profile at 2.6 GHz with a 60 dB dynamic range. (a) RT generated channel. (b) Pre-processed channel with 12 taps and 5 ns tap spacing using the proposed approach. (c) Rounding delays approach with 12 taps and 5 ns tap spacing. (d) Emulated pre-processed channel with 12 taps and 20 ns tap spacing setting on the emulator.

an average FRAC of 0.73 and 0.37 in the LoS and NLoS time instances, respectively. Nonetheless, it can be observed that the magnitude of the dominant Doppler frequency components in the emulated Doppler profile in Fig. 13(d) is reproduced relatively well, despite the difference in tap spacing between the emulated and pre-processed channels. This is because the magnitude of the individual Doppler frequency components remain relatively unchanged despite the shift along the Doppler frequency axis. However, the tap spacing change has a significant impact on the phase of the Doppler frequency components which results in a reduced similarity of the emulated Doppler profile to the RT simulated Doppler profile as shown in Fig. 14.

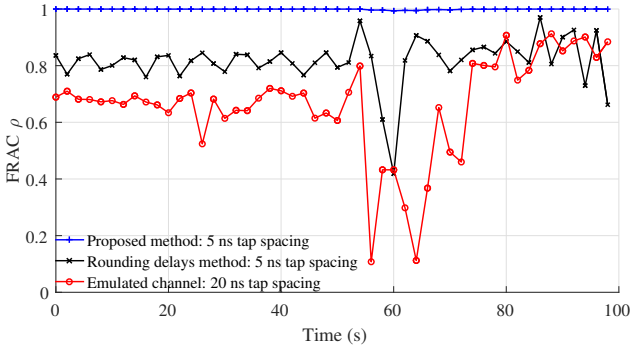

Fig. 14. Similarities of the emulated and the pre-processed channels' Doppler profile with 12 taps to the Doppler profile of the RT channel at 2.6 GHz. The emulated channel has a 20 ns tap spacing and the pre-processed channels have a 5 ns tap spacing.

VI. CONCLUSION

In this paper, a framework for delay alignment and tap selection has been proposed for pre-processing site-specific measured or RT simulated radio channels for hardware emulation with high-fidelity preservation of the CFR. The delay alignment process was formulated as an FIR filter design problem for approximating the ideal FD filter. The minimax FIR filter was shown to be robust for this purpose. In addition, it was shown for this convex optimization based approach of FIR filter design, delay drifts across the time and antenna pairs can be easily modified by simply adding an affine constraint to the optimization problem. This facilitates finding the optimal solution for a given hardware specification.

By selecting a suitable filter length and exploiting the resulting sparsity in the delay domain of each channel snapshot, the tap selection process was formulated as a sparse approximation problem. OMP was used in the second stage of tap selection, where the stopping condition was determined by the number of taps supported by a particular hardware configuration.

The advantage of file-based digital channel emulators in the preserving site-specific channels for playback in the laboratory is thus two-fold. First, they allow the use of optimal tap-delay alignment and selection processes that would not be possible in a real-time application due to their iterative nature. Second, site-specific measured or RT simulated channels can be independently generated and later replayed in real-time. In the presence of measurement uncertainties and imperfect hardware, poor pre-processing strategies were observed to be the main

contributors of errors in the emulated CFR in state-of-the-art channel emulators.

ACKNOWLEDGMENT

The authors would like to thank Prof. M. G. Christensen for the fruitful and insightful discussions.

REFERENCES

[1] J. Sozanski and T. Grosch
Radio Frequency Multipath Channel Emulation System and Method
U.S. Patent US9 130 667B2, Sep 8, 2015.

[2] J. J. Olmos, A. Gelonch, F. J. Casadevall, and G. Femenias
Design and Implementation of a Wide-Band Real-Time Mobile Channel Emulator
IEEE Trans. Veh. Technol., vol. 48, no. 3, pp. 746–764, 1999.

[3] J. Cao *et al.*
Design and Verification of a Virtual Drive Test Methodology for Vehicular LTE-A Applications
IEEE Trans. Veh. Technol., vol. 67, no. 5, pp. 3791–3799, 2018.

[4] J. Cao, F. Tila, and A. Nix
Design and Implementation of a Wideband Channel Emulation Platform for 5G mmWave Vehicular Communication
IET Communications, vol. 14, pp. 2369–2376(7), August 2020.

[5] R. K. Sharma *et al.*
Over-the-Air Testing of Cognitive Radio Nodes in a Virtual Electromagnetic Environment
Int. J. Antennas Propag., vol. 2013, 2013.

[6] P. Kyösti, L. Hentilä, W. Fan, J. Lehtomäki, and M. Latva-Aho
On Radiated Performance Evaluation of Massive MIMO Devices in Multiprobe Anechoic Chamber OTA Setups
IEEE Trans. Antennas Propag., vol. 66, no. 10, pp. 5485–5497, 2018.

[7] Y. Ji *et al.*
Virtual Drive Testing Over-the-Air for Vehicular Communications
IEEE Trans. Veh. Technol., vol. 69, no. 2, pp. 1203–1213, 2020.

[8] P. Huang, M. J. Tonnemacher, Y. Du, D. Rajan, and J. Camp
Towards Massive MIMO Channel Emulation: Channel Accuracy Versus Implementation Resources
IEEE Trans. Veh. Technol., vol. 69, no. 5, pp. 4635–4651, 2020.

[9] M. Wickert and J. Papenfuss
Implementation of a Real-Time Frequency-Selective RF Channel Simulator Using a Hybrid DSP-FPGA Architecture
IEEE Trans. Microw. Theory Techn., vol. 49, no. 8, pp. 1390–1397, 2001.

[10] A. Alimohammad and B. F. Cockburn
Modeling and Hardware Implementation Aspects of Fading Channel Simulators
IEEE Trans. Veh. Technol., vol. 57, no. 4, pp. 2055–2069, 2008.

[11] J. Mar, C.-C. Kuo, Y.-R. Lin, and T.-H. Lung
Design of Software-Defined Radio Channel Simulator for Wireless Communications: Case Study With DSRC and UWB Channels
IEEE Trans. Instrum. Meas., vol. 58, no. 8, pp. 2755–2766, 2009.

[12] Q. Zhu *et al.*
A Novel 3D Non-Stationary Wireless MIMO Channel Simulator and Hardware Emulator
IEEE Trans. Commun., vol. 66, no. 9, pp. 3865–3878, 2018.

[13] M. Hofer *et al.*
Real-Time Geometry-Based Wireless Channel Emulation
IEEE Trans. Veh. Technol., vol. 68, no. 2, pp. 1631–1645, 2019.

[14] Q. Zhu, Z. Zhao, K. Mao, X. Chen, W. Liu, and Q. Wu
A Real-Time Hardware Emulator for 3D Non-Stationary U2V Channels
IEEE Trans. Circuits Syst. I, vol. 68, no. 9, pp. 3951–3964, 2021.

[15] F. Kaltenberger, G. Steinbock, G. Humer, and T. Zemen
Low-Complexity Geometry Based MIMO Channel Emulation
In *Proc. 1st Eur. Conf. Antennas Propag.*, 2006, pp. 1–8.

[16] F. Kaltenberger, T. Zemen, and C. W. Ueberhuber
Low-Complexity Geometry-Based MIMO Channel Simulation
EURASIP J. Adv. Signal Process., vol. 2007, 2007.

[17] A. W. Mbugua, Y. Chen, and W. Fan
On Simplification of Ray Tracing Channels in Radio Channel Emulators for Device Testing
In *Proc. 15th Eur. Conf. Antennas Propag.*, 2021, pp. 1–5.

[18] T. Laakso, V. Valimaki, M. Karjalainen, and U. Laine
Splitting the Unit Delay [FIR/All Pass Filters Design]
IEEE Signal Process. Mag., vol. 13, no. 1, pp. 30–60, 1996.

[19] C. Mehlfuhrer and M. Rupp
Approximation and Resampling of Tapped Delay Line Channel Models with Guaranteed Channel Properties
In *Proc. IEEE Int. Conf. Acoustics, Speech Signal Process.*, 2008, pp. 2869–2872.

[20] C. Mehlfuhrer, M. Rupp, and G. H. F. Kaltenberger
Low-Complexity MIMO Channel Simulation by Reducing the Number of Paths
In *Proc. ITG/IEEE Workshop Smart Antennas*, 2007.

[21] Y. S. Cho, J. Kim, W. Y. Yang, and C. G. Kang
MIMO-OFDM Wireless Communications with Matlab. 2 Clementi Loop, #02-01, Singapore 129809: John Wiley & Sons (Asia) Pte Ltd, 2010, ch. 2, sec. 2.2.4.2, pp. 63–65.

[22] A. W. Mbugua, Y. Chen, and W. Fan
Radio Channel Emulation for Virtual Drive Testing with Site-Specific Channels
In *Proc. 16th Eur. Conf. Antennas Propag.*, 2022, pp. 1–5.

[23] Keysight Technologies
PROPSIM F64, Radio Channel Emulator F8800A, 2021. [Online]. Available: https://www.keysight.com/gb/en/assets/7018-06665/data-sheets/5992-4078.pdf

[24] L. Karam and J. McClellan
Complex Chebyshev Approximation for FIR Filter Design
IEEE Trans. Circuits Syst. II: Analog Digit. Signal Process., vol. 42, no. 3, pp. 207–216, 1995.

[25] R. Crochiere and L. Rabiner
Interpolation and Decimation of Digital Signals—A Tutorial Review
Proc. IEEE, vol. 69, no. 3, pp. 300–331, 1981.

[26] T. N. Davidson
Enriching the Art of FIR Filter Design via Convex Optimization
IEEE Signal Process. Mag., vol. 27, no. 3, pp. 89–101, 2010.

[27] J. Kemppainen, T. Poutanen, and J. Harju
Method and Apparatus for Simulating Radio Channel
U.S. Patent US20 050 008 109A1, Jan 13, 2015.

[28] S. Schmidt
Measuring Device and Method with Efficient Channel Simulation
U.S. Patent US10 680 723B1, Jun 9, 2020.

[29] T. T. Cai and L. Wang
Orthogonal Matching Pursuit for Sparse Signal Recovery With Noise
IEEE Trans. Inf. Theory, vol. 57, no. 7, pp. 4680–4688, 2011.

[30] A. W. Mbugua, Y. Chen, L. Raschkowski, L. Thiele, S. Jaeckel, and W. Fan
Review on Ray Tracing Channel Simulation Accuracy in Sub-6 GHz Outdoor Deployment Scenarios
IEEE Open J. Antennas Propag., vol. 2, pp. 22–37, 2021.

[31] S. Jaeckel, L. Raschkowski, K. Börner, and L. Thiele
QuaDRiGa: A 3-D Multi-Cell Channel Model With Time Evolution for Enabling Virtual Field Trials
IEEE Trans. Antennas Propag., vol. 62, no. 6, pp. 3242–3256, 2014.

[32] T. Jämsä, T. Poutanen, and H. Hakalahti

Realization of a Multipath Radio Channel Simulator for Wideband Wireless Radio Systems
In *Proc. 7th Virginia Tech. Symp. Wireless Pers. Commun.*, 1997, pp. 1–11.

[33] Spirent
Spirent Vertex Channel Emulator. [Online]. Available: https://assets.ctfassets.net/wcxs9ap8i19s/1vGUSaaJZCNDi34PeCFgvr/c41cb9ced2f95a00e7c59d643dd6c69c/DS-Spirent-Vertex-Channel-Emulator.pdf

[34] W. Putnam and J. Smith
Design of Fractional Delay Filters Using Convex Optimization
In *Proc. Workshop Appl. Signal Process. Audio Acoust.*, 1997, pp. 4 pp.–.

[35] M. Grant and S. Boyd
CVX: Matlab Software for Disciplined Convex Programming, version 2.1
http://cvxr.com/cvx, Mar. 2014.

[36] M. Grant and S. Boyd
Graph Implementations for Nonsmooth Convex Programs
In *Recent Advances in Learning and Control*, ser. Lecture Notes in Control and Information Sciences, V. Blondel, S. Boyd, and H. Kimura, Eds. Springer-Verlag Limited, 2008, pp. 95–110.

[37] R. Luebbers
Finite Conductivity Uniform GTD Versus Knife Edge Diffraction in Prediction of Propagation Path Loss
IEEE Trans. Antennas Propag., vol. 32, no. 1, pp. 70–76, 1984.

[38] L. Thiele, S. Dai, M. Kurras, M. Lossow, L. Raschkowski, and S. Jaeckel
Multi-User Massive MIMO Properties in Urban-Macro Channel Measurements
In *Proc. 53rd Asilomar Conf. Signals, Syst. Comput.*, 2019, pp. 1091–1097.

[39] Christophe Seux
Blender Demo Files: Classroom. [Online]. Available: https://download.blender.org/demo/test/classroom.zip

[40] W. Heylen and S. Lammens
FRAC: A Consistent Way of Comparing Frequency Response Functions
In *Proc. Conf. Identification Eng. Syst.*, 1996, pp. 48–57.

[41] R. J. Allemang
The Modal Assurance Criterion – Twenty Years of Use and Abuse
Sound and Vibration, pp. 14–20, 2003.

[42] D. W. Hess
Historical Background on the Use of Equivalent Stray Signal in Comparison of Antenna Patterns
In *Proc. 5th Eur. Conf. Antennas Propag.*, 2011, pp. 2522–2526.

[43] A. Newell and G. Hindman
Antenna Pattern Comparison Using Pattern Subtraction and Statistical Analysis
In *Proc. 5th Eur. Conf. Antennas Propag.*, 2011, pp. 2537–2540.

Allan Wainaina Mbugua received the B.Sc. degree in telecommunication and information engineering from the Jomo Kenyatta University of Agriculture and Technology, Juja, Kenya, in 2014, and the M.Sc. degree in telecommunications engineering from the University of Cassino and Southern Lazio, Cassino, Italy, in 2018. He is currently pursuing the Ph.D. degree with Huawei Techonologies Duesseldorf GmbH, Munich Research Center, Munich, Germany and the Antennas, Propagation and Millimetre-wave Systems (APMS) Section, Aalborg University, Aalborg, Denmark. His current research interests include radio channel sounding, radio channel simulation, and radio channel emulation.

Yun Chen received the B.Sc. degree from the University of Duisburg-Essen, Germany in 2006, and the M.Sc. degree from the University of Duisburg-Essen, Germany in 2008, and the Ph.D. degree from the University of Duisburg-Essen, Germany in 2012. He was with Rohde & Schwarz and Fraunhofer research society, in Munich, Germany and is currently working as project manager with Huawei Technologies Duesseldorf GmbH, Munich, Germany with a focus on site-specific channel modelling and technologies research on 5G system testing.

Leszek Raschkowski received the Dipl.-Ing. (M.S.) degree in Electrical Engineering in 2012 from Technische Universität Berlin, Germany. Currently, he is employed as a research associate and project manager at Fraunhofer Heinrich Hertz Institute in Berlin, Germany. Leszek is working on several research projects in the field of wireless communications. In addition, he is actively contributing to 3GPP standardization work related to the radio access network as a regular delegate since 2013. At the moment, he works on the integration of non-terrestrial networks (satellite constellations) into the 5G ecosystem. His research interests include measuring, modeling and simulating radio propagation channels, as well as performance analysis of wireless communication systems. This encompasses 3D MIMO, deployments in industrial factory halls, aerial vehicles (drones) and satellites.

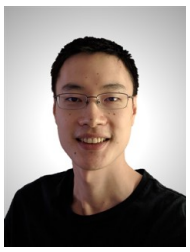

Yilin Ji received his B.Sc. degree in Electronics Science and Technology and M.Eng degree in Integrated Circuit Engineering from Tongji University, China, in 2013 and 2016, respectively. In 2021, he received his Ph.D. degree in Wireless Communications from Aalborg University, Denmark. He is currently a Post.Doc at the Antennas, Propagation and Millimeter-wave Systems (APMS) section at Aalborg University, Denmark. His main research areas are propagation channel characterization, and MIMO over-the-air testing.

Mohamed Gharba received the B.Sc. degree in telecommunications and electronics engineering from the Suez Canal University, Port-Said, Egypt, in 2006, the Master degree (Diplôme d'Ingénieur) in telecommunication and networks engineering from ENSEA (École Nationale Supérieure de l'Électronique et de ses Applications), Cergy, France, in 2008, and the Ph.D. degree in radiocommunication with Orange Labs, Cesson-Sévigné, France and the CNAM (Conservatoire national des arts et métiers), Paris, France in 2012. He is currently working as a principal engineer in 5G area, in Huawei Technologies Duesseldorf GmbH, Munich Research Center, Munich, Germany. His current research interests and activity include waveform, radio interference mitigation, and 5G radio for verticals (V2X, Industry and eHealth).

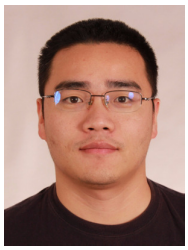

Wei Fan (Senior Member, IEEE) received the B.E. degree from the Harbin Institute of Technology, Harbin, China, in 2009, the master's double degrees (Hons.) from the Politecnico di Torino, Turin, Italy, and the Grenoble Institute of Technology, Grenoble, France, in 2011, and the Ph.D. degree from Aalborg University, Aalborg, Denmark, in 2014. In 2011, he joined Intel Mobile Communications, Aalborg, as a Research Intern. He conducted a three-month internship with Keysight Technologies, Oulu, in 2014. He is currently an Associate Professor with the the Antennas, Propagation and Millimetre-wave Systems (APMS) Section, Aalborg University. His current research interests include over-the-air (OTA) testing of multiple antenna systems and radio channel sounding, parameter estimation, modeling, and emulation.